



Geophysical Research Letters

RESEARCH LETTER

10.1029/2018GL078321

Special Section:

Bridging Weather and Climate:
Subseasonal-to-Seasonal (S2S)
Prediction

Key Points:

- Lag correlations of the reconstructed OLR anomalies reveal that OMI represents northward and eastward propagation in boreal summer
- Intercomparison of the OLR anomalies from OMI, RMM, and two BSISO indices shows that they differ significantly in representing zonal and meridional propagation
- Phase composite on the intraseasonal indices is not reliable in estimating propagation

Supporting Information:

- Supporting Information S1

Correspondence to:

S. Wang,
sw2526@columbia.edu

Citation:

Wang, S., Ma, D., Sobel, A. H., & Tippett, M. K. (2018). Propagation characteristics of BSISO indices. *Geophysical Research Letters*, 45, 9934–9943. <https://doi.org/10.1029/2018GL078321>




Received 13 APR 2018

Accepted 25 JUL 2018

Accepted article online 1 AUG 2018

Published online 19 SEP 2018

Propagation Characteristics of BSISO Indices

Shuguang Wang¹ , Ding Ma¹, Adam H. Sobel^{1,2} , and Michael K. Tippett¹ 

¹Department of Applied Physics and Applied Mathematics, Columbia University, New York, NY, USA, ²Lamont-Doherty Earth Observatory of Columbia University, Palisades, NY, USA

Abstract The spatial structure and propagation of tropical intraseasonal convection anomalies diagnosed with the outgoing longwave radiation-based Madden-Julian Oscillation index are examined in the boreal summer and winter seasons. It is shown that the outgoing longwave radiation-based Madden-Julian Oscillation index represents both northward and eastward propagation in summer and eastward propagation in winter in a manner consistent with Madden-Julian Oscillation and Boreal Summer Intraseasonal Oscillation propagation as diagnosed in many previous studies. The outgoing longwave radiation-based Madden-Julian Oscillation index and three other widely used indices for tracking the Boreal Summer Intraseasonal Oscillation are then compared in their lag correlation structure over selected reference areas, cross-correlation coefficients of the two principal component time series, and time-dependent phase angle composites. The outgoing longwave radiation anomalies from these different indices propagate differently according to these diagnostics. One of them exhibits little propagation at all, even though one would expect good propagation based on composites of the phases separately. This illustrates the general point that while composites of individual phases, presented in a sequence, are generally taken to imply that the phases tend to occur in that sequence in time, that need not be the case. It is suggested that propagation characteristics are relevant to the application of the indices and that smoother propagation is desirable.

Plain Language Summary The tropical intraseasonal oscillation is a large-scale pattern of cloud and circulation in the equatorial regions recurring every 30 to 60 days. The pattern propagates both northward and eastward in the northern summer season, and brings a large amount of rain and disturbed weather along its path. To track its movement, scientists have developed simple indices using winds and the energy radiating from the Earth as seen from satellites. Here we examine how well these indices accurately track the oscillation by looking into a large number of historical events, and show that our diagnostics may further help improve these indices.

1. Introduction

Tropical intraseasonal oscillations, including the Madden-Julian Oscillation (MJO) and Boreal Summer Intraseasonal Oscillation (BSISO), are primary modes of climate variability in the deep tropics on intraseasonal time scales. The MJO in northern winter is characterized by slow eastward propagation around the equator. Propagation of the BSISO is more complex. Wang and Rui (1990) found that convection in boreal summer exhibits propagation in the Indian Ocean from equator to ~20°N on intraseasonal time scales, and suggested that this northward propagation of convection is distinct from the eastward propagating MJO identified by Madden and Julian (1971). Zhu and Wang (1993) also noted a significant standing component in BSISO. On the other hand, Lawrence and Webster (2002) analyzed ~60 such events, and found that most BSISOs have both northward and eastward propagation. In light of these findings, we take both northward and eastward propagation as defining characteristics of tropical intraseasonal oscillations in the boreal summer, while acknowledging that BSISO sometimes also has westward propagating and standing components.

A number of authors have developed indices to represent the temporal and spatial structures of convection and circulation associated with the BSISO. Kikuchi et al. (2012, hereafter K12) and Kiladis et al. (2014, K14 hereafter) developed outgoing longwave radiation (OLR)-based indices using slightly different techniques. Besides differences in seasonality, these two indices also overcame some issues with the widely used MJO real-time multivariate MJO index (RMM; Wheeler & Hendon, 2004), which weights wind anomalies much more than OLR anomalies (e.g., Straub, 2013). Another widely used BSISO index applicable to the Indo-Pacific region was developed by Lee et al. (2013, L13 hereafter). These authors have carefully demonstrated in variety of ways that these indices are representative of intraseasonal oscillations. They have shown, for

example, that the indices explain sufficient fractions of the variances in the total fields and that they have intraseasonal peaks in their power spectra.

Because these indices for tropical intraseasonal oscillations potentially have wide applications in climate monitoring and subseasonal forecasts, their properties have received scrutiny to assess their value in different situations and applications. Their propagation characteristics, on the other hand, have been less thoroughly examined compared to other properties. Propagation is often addressed by visual inspection of the structures composited upon their phases. The assumption that one phase follows the next sequentially in time is generally implicit, but is not actually guaranteed for individual events or in real time by the construction of the composites. Here we address the issue of propagation more completely, using several diagnostics that explicitly account for the temporal sequencing of anomalies associated with different phases of each index. We limit our analysis to the above three publicly available BSISO indices and RMM. We do not address BSISO indices developed by other authors (e.g., Lee & Wang, 2016; Lin, 2013; Sabeerali et al., 2017; Suhas et al., 2013) but suggest that it would be useful to apply the diagnostics here to those as well.

Our primary focus is the OLR MJO index (OMI). K14 developed their OMI for all seasons. K14 studied some properties of OMI in winter and suggested that the OMI is appropriate if convection is of primary interest. K14 did not explore to what extent the OMI index can faithfully represent propagation and structure of the BSISO, nor how it differs from several other indices for BSISOs. We will show that OMI represents both northward and eastward propagation of intraseasonal convection in summer, capturing the BSISO in a manner faithful to the picture obtained from previous studies using a wide range of other methods.

2. Methods and Data

The intraseasonal oscillations indices (RMM, K12, L13, and OMI) are all daily indices based on eigenvalue analysis of the data matrix constructed from the spatial and temporal distribution of tropical convection and/or circulation. The principal components are taken as the indices for diagnosis of phase, amplitude, spectral characteristics, and other properties (see supporting information for a summary of these indices). Among them, K12 and OMI are exclusively convection indices, while RMM and L13 are multivariate indices. The BSISO index by L13 that we analyze here is the one referred to as BSISO1 in that study, which derived multiple indices. K14 applies standard empirical orthogonal function (EOF) analysis to OLR but restricts their analysis to data within a 121-day sliding window in all years to construct EOFs that change each day of the year, so that the OMI is applicable in all seasons. The resultant EOFs have both zonal and meridional structures. The explained variance varies with seasons in a relatively narrow range: 26–33% (Figure 1 of K14). The bivariate correlation coefficient between OMI and RMM is highest (0.75) in December to February and lowest (0.63) in June to August (Table 2 in K14), indicating substantial difference between the two in the summer.

To characterize propagation associated with these indices, we compute the lag correlation of each index with OLR anomalies over several representative reference areas. We use the NOAA interpolated daily 2.5 resolution OLR data set (Liebmann & Smith, 1996) from 1979 to 2016. Two types of OLR anomalies, both as a function of time, longitude, and latitude, are computed: (i) band-pass filtered OLR anomalies with cutoff periods of 20 and 90 days and (ii) reconstructed OLR anomalies, R , computed as the product of the PC time series and the two leading OLR EOFs:

$$R = PC1(t) \times EOF1 + PC2(t) \times EOF2,$$

where t denotes time, PCs are the principle component time series, and EOFs denote the empirical orthogonal functions. The RMM EOFs are functions of longitude; the K12 and L13 EOFs are functions of longitude and latitude. The OMI EOFs are functions to latitude, longitude, and the date of year.

Since RMM EOFs have no latitudinal extent, the RMM OLR anomalies are estimated at each grid point by regressing band-pass-filtered OLR anomalies onto the RMM PC time series using multiple linear regression with PC1 and PC2 as the predictors. This regression approach for reconstruction is appropriate since PC1 and PC2 are orthogonal as required by the EOF analysis. As a result, the reconstructed RMM OLR anomalies are a function of time, longitude, and latitude, as desired. We will compute the lag correlation of these OLR anomalies against each BSISO index for boreal summer (May to October), omitting off-season data.

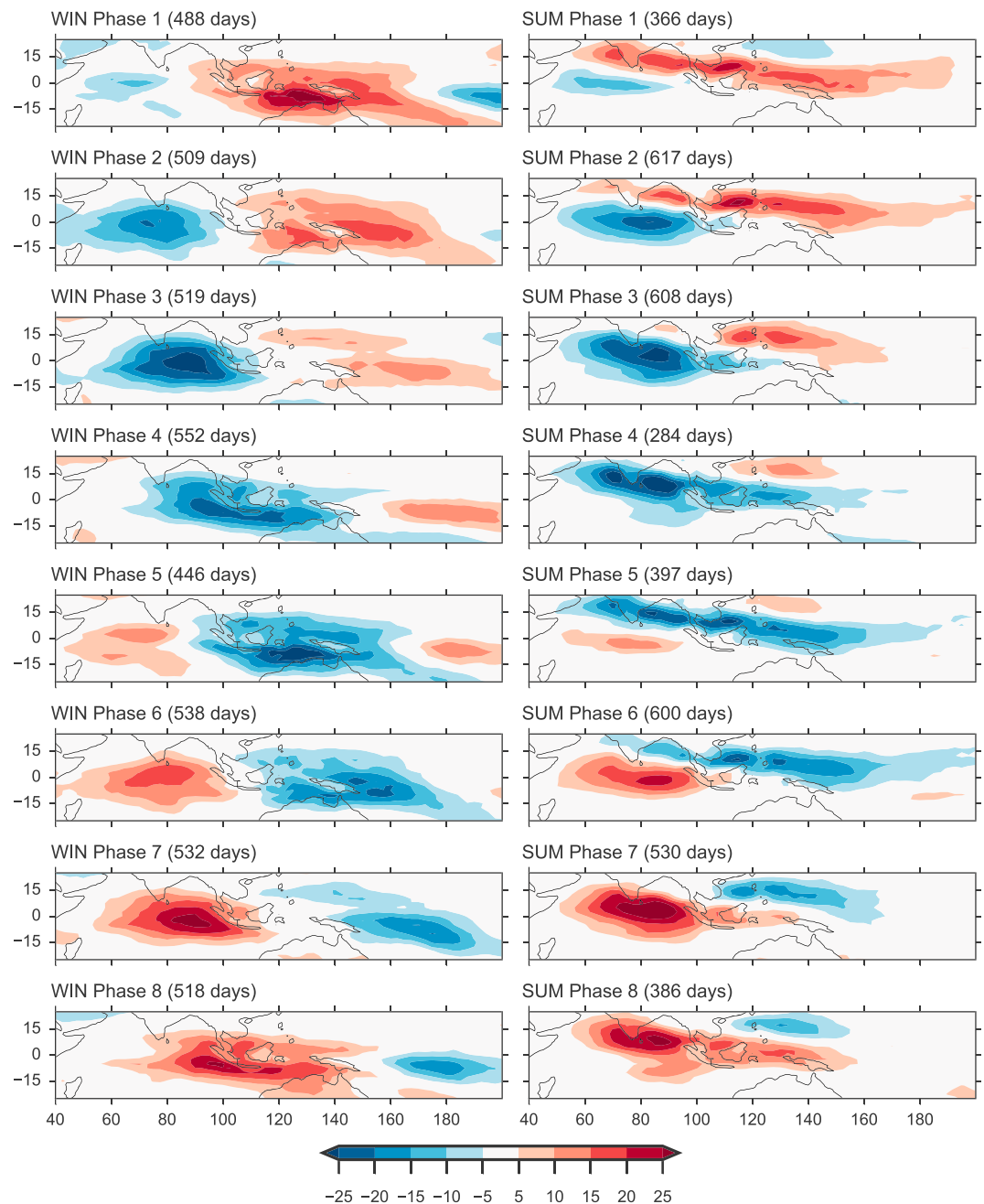


Figure 1. Band-pass-filtered OLR anomalies (W/m^2) composited on the OMI index from (left column) November to April and (right column) May to October.

3. Results

We first compare the OMI index in boreal winter (December to March) to that in summer (May to October). Figure 1 shows band-pass-filtered OLR anomalies composited on eight different OMI phases in the summer and winter seasons. The OMI phase angles are computed as $\arctan(-OMI1/OMI2)$, where OMI1 and OMI2 are the two leading principal components of OMI. This winter composite indicates that the intraseasonal convection starts in phase 1 in the Indian Ocean, gradually strengthens and achieves maximum amplitude in the eastern Indian Ocean in phase 3, broadens over the southern Maritime Continent in phases 4 and 5, and weakens over the western Pacific Ocean during phases 6–8. The structure in summer differs from that in winter: a northwest-southeast tilted pattern is present in nearly all phases in summer, and there is northward

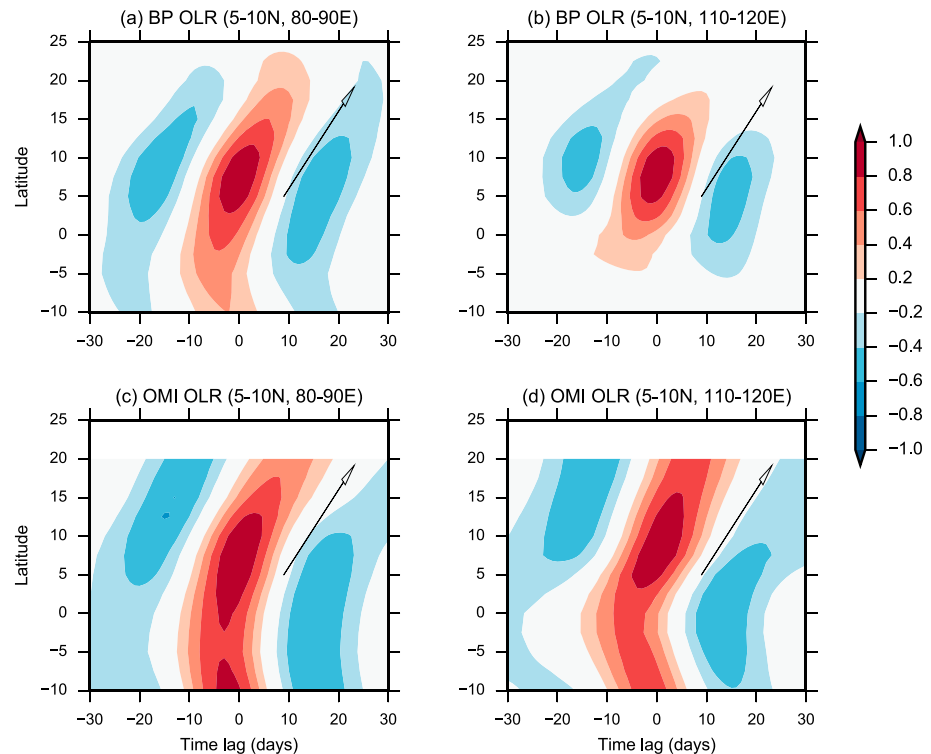


Figure 2. (top) Lag correlation of band-pass-filtered (20–70-day) OLR anomalies averaged over 80–90°E (a) and 110–120°E (b) in summer (May to October) against the same band-pass-filtered OLR anomalies averaged over the reference areas in IO and MC as indicated in the title of each panel. (bottom) Same as top but for OMI reconstructed OLR anomalies. Arrows indicate northward propagation speed of 1°/day.

as well as eastward movement. It thus appears that the composite patterns in both boreal winter and summer are similar to those based on the widely used RMM index (MJO life cycle composite from the MJO working group diagnostics; http://climate.snu.ac.kr/mjo_diagnostics/index.htm), and one might argue that the OMI does not offer more much than RMM in terms of propagation. However, as shown below, inferring propagation from composite may be misleading because the composites do not explicitly take time evolution into account. Presenting them in a sequence with increasing phase angle implies that the phases actually do occur sequentially in time, but this is not guaranteed for individual events or in real time. We diagnose the propagation directly below with a simple lag correlation analysis of reconstructed OLR anomalies, as well as lag correlations and time-dependent composites of phase angle constructed directly from the indices.

Figures 2a and 2b show the lag correlation of the band-pass-filtered OLR anomalies averaged over the same longitude range as the reference areas (80–90°E in a, 110–120°E in b) against the corresponding OLR anomalies over reference areas in the Indian Ocean (IO; averaged over the area 5–10°N, 80–90°E) and the Maritime Continent (MC; 5–10°N, 110–120°E). Consistent with the band-pass-filtered anomalies, the reconstructed OLR anomalies (Figures 2c and 2d) show northward propagation with a speed of $\sim 1^\circ$ per day. The reconstructed anomalies are less damped in time and latitude than are the band-passed anomalies, because intraseasonal noise is removed in the projection onto the leading two EOF modes of the OMI, allowing longer persistence in the reconstructed OLR anomalies. There is no northward propagation when the same lag correlation is computed in winter season (not shown).

In addition to northward propagation in summer, lag correlation of OLR anomalies at the equator (Figure 3) shows coherent eastward propagation at a speed of ~ 5 m/s in both summer and winter for reference areas in the IO (averaged over the area 10°S–10°N, 80–90°E) and MC (10°S–10°N, 110–120°E), similar to canonical MJO events in winter represented by the RMM index (not shown). Band-pass-filtered OLR anomalies barely persist through the MC in these results; unlike what is done in the construction of OMI, no filtering for eastward propagating components was applied to these data. The phase speed derived from lag correlations is similar in

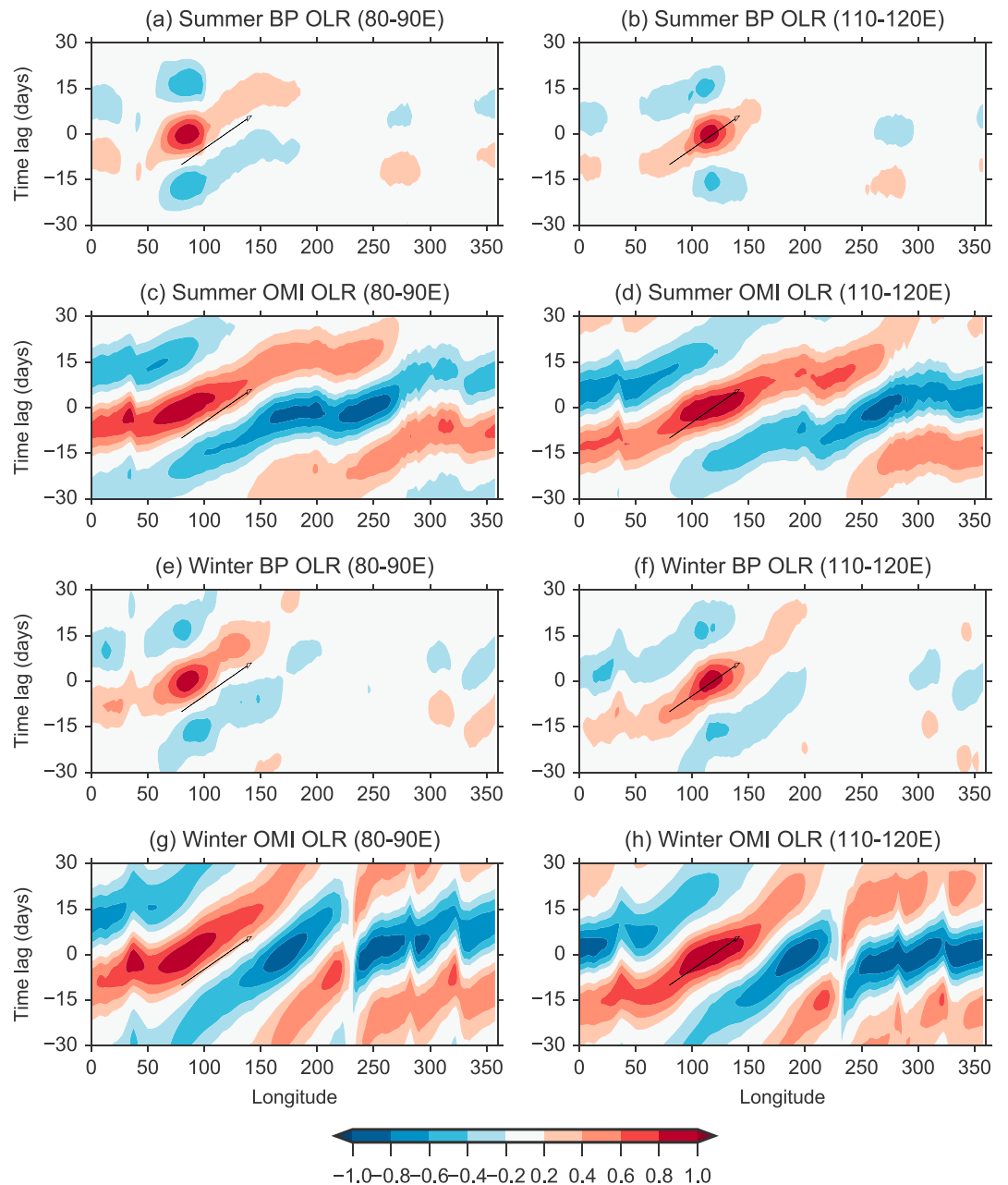


Figure 3. (a and b) Lag correlation of 20–90-day band-pass-filtered OLR anomalies averaged 10°S–10°N against the same OLR anomalies at two reference areas for OLR anomalies in summer. (c and d) Same as in (a) and (b) but for OMI reconstructed OLR anomalies. (e–h) Same as in (a)–(d) but for winter. The latitude range of the reference areas is 10°S–10°N. The longitude range of the reference areas is indicated in the title.

winter and summer, as indicated with the arrows indicating a speed of 5 m/s. OMI-reconstructed OLR anomalies have slightly faster eastward speed in summer, and the blocking by the MC in summer is less obvious. Despite these subtle differences in season and phase speed, we conclude that the OMI-reconstructed OLR anomalies represent coherent eastward propagation.

As discussed in section 1, propagation characteristics have been used to distinguish the MJO and BSISO in summer: the BSISO propagates in the meridional/zonal direction, while the MJO propagates only zonally. Here we compare these indices using bivariate correlation coefficient for the boreal summer (May to October). The correlation coefficient is 0.76 between OMI and K12 and 0.61 between OMI and RMM. The

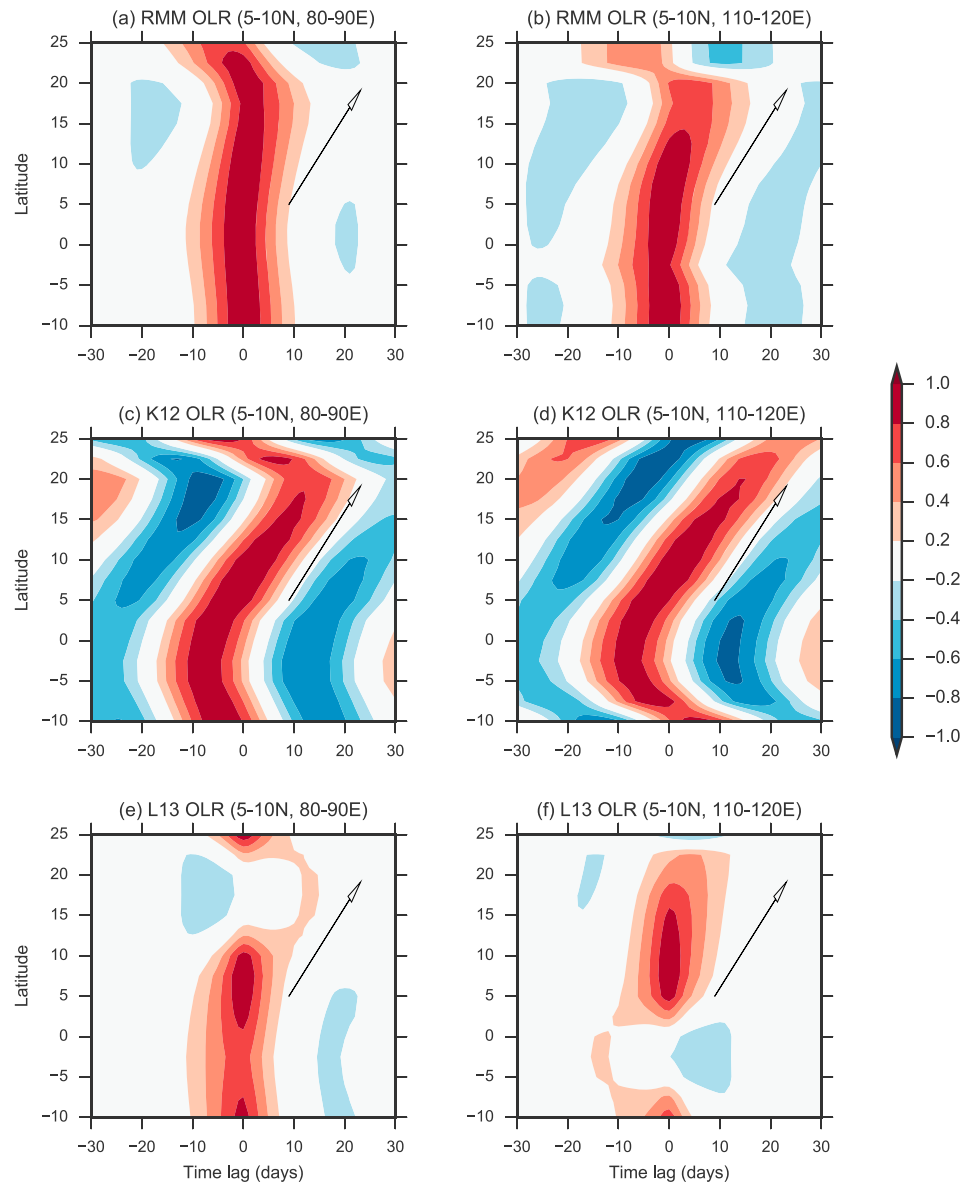


Figure 4. Same as Figures 2c and 2d but for lag correlation of the reconstructed OLR anomalies for (top) RMM, (middle) K12, and (bottom) L13 for the reference area in the (left panels) eastern Indian Ocean or (right panels) Maritime Continent.

higher correlation between OMI and K12, indicating that OMI can explain nearly 60% of the variance of K12, may be due to the fact that both OMI and K12, unlike RMM and L13, apply band-pass filtering to OLR. The correlation coefficient is relatively low (0.47) between K12 and L13, and (0.52) between OMI and L13, which is consistent with the lack of northward propagation in L13, as also shown below. Table S1 in supporting information summarizes these values.

As shown in K12 and L13, composites over the eight phases of the two indices are broadly similar in their spatial structures in the Indo-Pacific regions. (The phase composites are reproduced in the supporting information.) Here we show that this broad pattern match is not a sufficient condition for the two indices to have similar propagation characteristics. For reference, we first examine RMM. Figures 4a and 4b show lag correlation of the reconstructed OLR anomalies with both components of RMM through the multiple linear regression. There is no sign of northward propagation over the Indian Ocean, and only slow propagating signals north of 10°N in the Maritime Continent. This lack of northward propagation in RMM is not surprising since the EOFs of RMM have no latitudinal structure by construction. On the other hand, the K12 and L13 BSISO

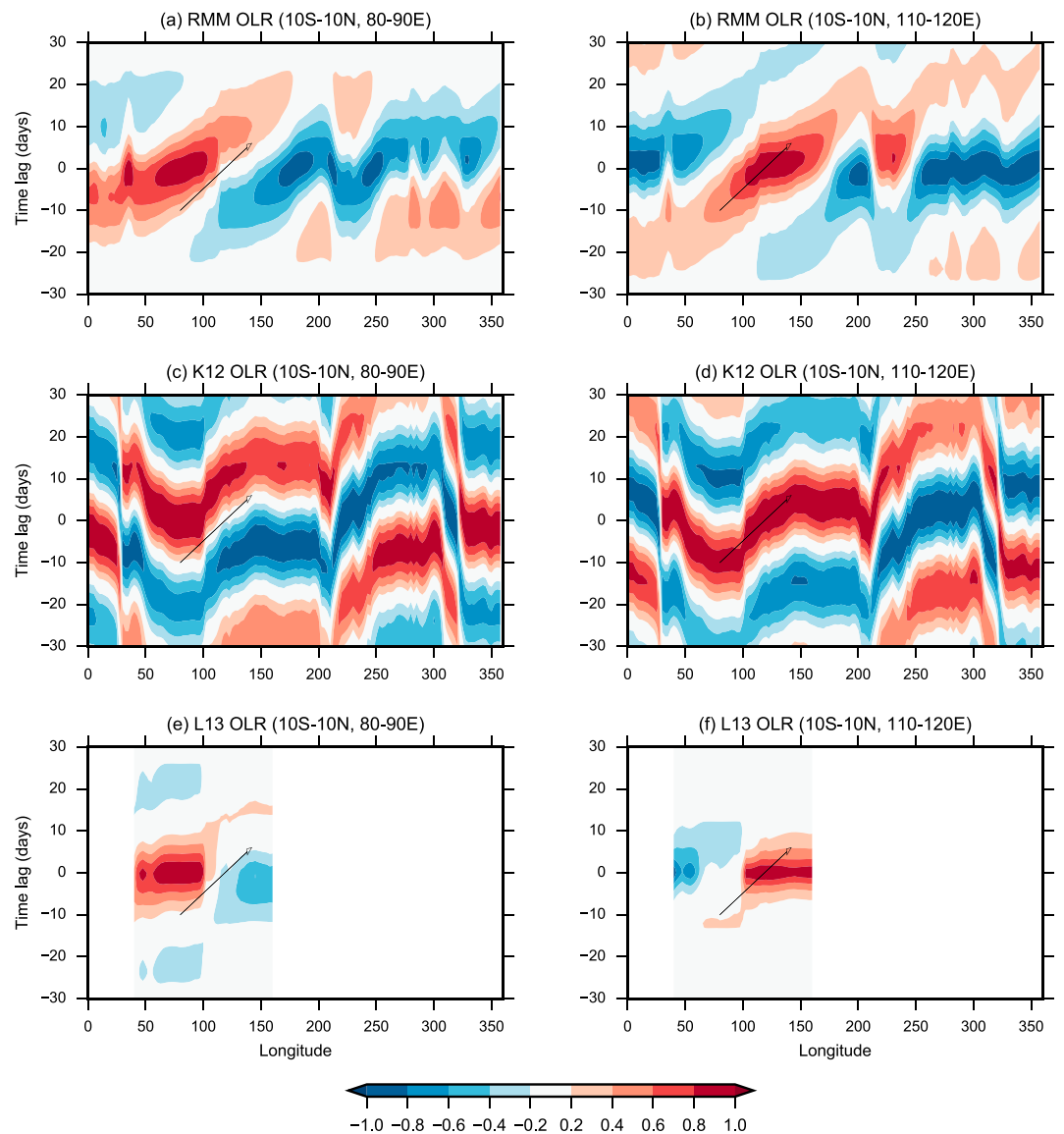


Figure 5. Same as in Figures 3c and 3d but for lag correlation of the regressed OLR anomalies from (a and b) RMM and reconstructed OLR anomalies from (c and d) K12 and (e and f) L13. The blank area in the bottom panels is present because the L13 is a regional index (40–180°E). The reference area is indicated in the title of each panel.

indices were constructed specifically to track northward propagation. Figure 4 shows lag correlation of reconstructed OLR anomalies for the BSISO indices in K12 and L13. Consistent northward propagation is evident for K12 in the lag correlation for OLR anomalies over the two reference areas, similar to the lag correlation of OMI (Figure 2), but little northward propagation can be identified from L13 OLR anomalies (Figures 4c and 4d). The lag correlation patterns of L13 (Figures 4c and 4d) do indicate a standing wave, consistent with earlier observation that the BSISO has a significant standing component between the equatorial Indian Ocean and Philippine Sea (Zhu & Wang, 1993).

Zonal propagation can also be estimated from lag correlation of the reconstructed OLR anomalies. For reference, we first examine the lag correlation patterns of regressed RMM OLR anomalies. Figures 5a and 5b show clear eastward propagation in the Indian Ocean and western Pacific. Lag correlation applied to EOF-reconstructed RMM OLR anomalies (without meridional structure) shows a similar pattern (not shown), indicating that reconstructing OLR anomalies from multiple linear regression is effective. The lag correlation pattern from K12 shows clear eastward propagation eastward of the reference areas (Figures 5c and 5d) to the

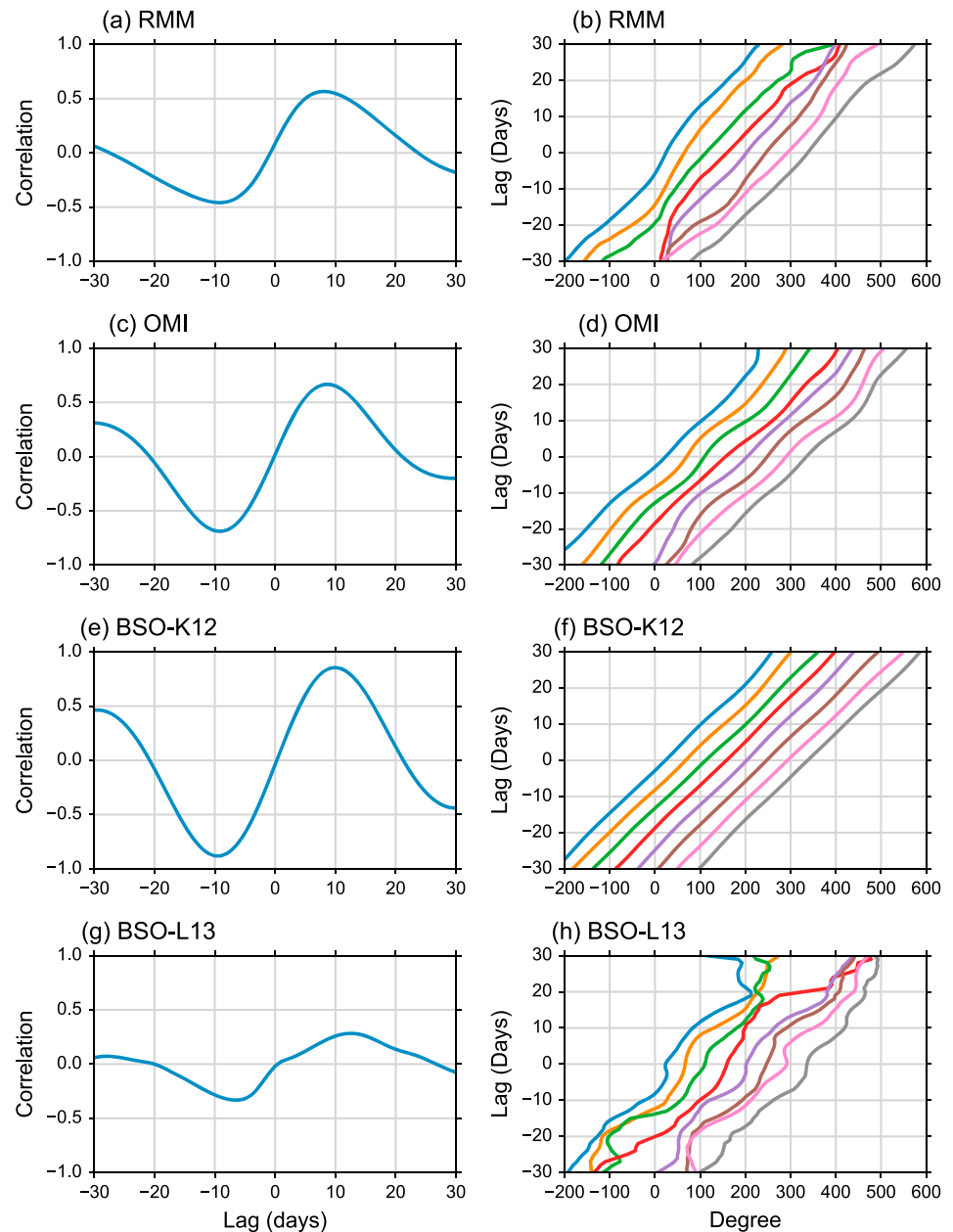


Figure 6. (left) Cross lag correlation coefficient of PC1 and PC2 for RMM, OMI, K12, and L13. (right) Composite of angles at day 0 within every 45° bins (0–45°, 45–90°, ..., 315–360°) with amplitude greater than 1 at day 0.

central Pacific Ocean, but nearly stationary structure immediately 10° westward of the reference area, and westward propagation further to the west. The westward propagation is also an observed feature of BSISO (e.g., Lawrence & Webster, 2002). OMI does not capture the westward propagation because only the eastward propagating component is preserved by their band-pass filter (Kiladis et al., 2014). On the other hand, L13 shows a standing wave pattern, with little zonal propagation (Figures 5e and 5f). We have also inspected the temporal and spatial structures of reconstructed OLR anomalies for multiple individual years (not shown), and the results from that support the conclusions drawn above about the propagation based on the lag correlation analyses presented here.

The preceding results are based on lag correlation of OLR fields over two reference areas. Phase propagation can also be diagnosed using the indices alone, by checking to what extent the index phases tend to proceed in sequence. This avoids any need to select a reference area or reconstruct the OLR field. A caveat is that these

indices do not all use the same meteorological variables: RMM and L13 differ from the others in that they contain information from both zonal wind and OLR. The left panels in Figure 6 show the lag correlation between PC1 and PC2 for RMM, OMI, K12, and L13. In principle, PC1 and PC2 should be orthogonal by construction, meaning the correlation coefficient is near zero at lag day 0. This is well satisfied except for RMM. The seeming lack of orthogonality in RMM is due to seasonality: the correlation coefficient is indeed near zero at lag day 0 if all-season RMM time series are used. The lag correlation coefficient is antisymmetric with respect to time lag in OMI and K12, but less so in L13. The maximum value of the lag correlation coefficient is 0.57 for RMM, 0.66 for OMI, and 0.88 for K12, but only 0.28 for L13. OMI and K12 reach their maximum values at lag days 9–10, indicating that the propagating modes represented by PC1 and PC2 in quadrature have a period of 36–40 days, while L13 reaches its maximum at day 13 and its minimum value at day 6. The relatively weak lag correlation coefficient from L13 is consistent with the poor propagation inferred from lag correlation of reconstructed anomalies at different reference areas above (Figures 4 and 5).

We further characterize propagation in the PC phase space by the phase angle defined by the two principal components. The right panels in Figure 6 show the phase angles of these indices composited on *lag day 0* (amplitude greater than 1), averaged over eight initial phase ranges (0–45°, 45–90°, ..., 315–360°) for all the four indices. The average phase angle Θ in each phase range is written as

$$\Theta = \arctan\left(\frac{1}{N} \sum_k \sin\theta_k, \frac{1}{N} \sum_k \cos\theta_k\right),$$

where k is the index of the occurrence. Averaging after taking sine or cosine is necessary to avoid artifacts of phase wrapping (i.e., jumping from 2π to 0). Propagation from one phase to the next with constant speed in phase space corresponds to straight lines, and wiggles indicate that the propagation represented by the index is noisy or sampling variability. L13, RMM, OMI, and K12 have increasingly more coherent propagation, in the same order as the lag correlation in the left panels of Figure 6.

4. Conclusion

We have examined some properties of the OLR-based MJO index (OMI). The spatial structure and propagation in boreal summer, in particular, is compared to that in winter. Lag correlation analysis of the OLR anomalies projected on eigenvectors associated with OMI in summer shows both northward and eastward propagation in summer on intraseasonal time scale, suggesting that the OMI can be used for monitoring and prediction of the Boreal Summer Intraseasonal Oscillation (BSISO).

Lag correlation of reconstructed OLR fields against the indices, lag correlation of the principal components of the indices themselves, and time-dependent phase angle composites are further employed to compare propagation in OMI and another three widely used indices for tropical intraseasonal oscillations. This comparison reveals that these indices differ significantly in the degree to which they represent northward and eastward propagation. While the propagation characteristics of the various BSISO indices may be taken as implicit in composites of the individual phases labeled by numbers (phases 1, 2, etc.), the implication that the phases generally occur in that sequence may be contradicted by lagged correlations calculated using reconstructions of the OLR field from each index. The RMM index does not capture northward propagation, as expected. The BSISO index by Kikuchi et al. (2012) has coherent northward propagation over the Indian Ocean and Maritime Continent, with both eastward and westward propagation, while the BSISO index by Lee et al. (2013) shows standing wave characteristics, with little northward and eastward propagation. These results are not completely consistent, especially for L13, with the propagation implied from standard phase composites, whose construction does not take time evolution into account. Our tests indicate the use of U850, and the time windows used to compute the EOFs contribute to the lack of northward propagation in L13 (supporting information). The OMI has higher bivariate correlation with the BSISO index (Kikuchi et al., 2012) than does the MJO RMM index. We conclude that the OMI represents both eastward and northward propagation of convection in summer to a greater degree than do the other ISO indices we have examined.

While our study focuses on propagation characteristics, we emphasize that each index has its own advantages and disadvantages. Both RMM and L13 track the circulation associated with MJO or BSISO when convection is weak, while OMI and K12 is better suited for tracking MJO/BSISO convection. The value of the

RMM and L13 indices also lies in their application in real-time monitoring and forecast without any need for band-pass filtering. For the same reason, OMI and K12 cannot be directly used for these purposes. To overcome this issue, Kikuchi et al. (2012) and Kiladis et al. (2014) developed real-time versions of their respective indices, in which the OLR data are first processed using time window techniques and further projected onto the EOFs obtained using band-pass-filtered data. Our lag correlation diagnostics (Figures S5 and S6 in the supporting information) indicate that the real-time versions share the same propagation characteristics derived from the lag correlation diagnostics as the band-pass-filtered versions. In light of the above discussion, we recommend that judicious use of these indices should take into account of their propagation characteristics, as well as their other advantages and disadvantages.

Acknowledgments

S.W. and A.H.S. acknowledge support from NSF AGS-1543932 and ONR N00014-16-1-3073. This research has been conducted as part of the NOAA MAPP S2S Prediction Task Force and supported by NOAA grant NA16OAR4310076. We are grateful for the insightful comments by George N. Kiladis, Kazuyoshi Kikuchi, Matthew Wheeler, and Bin Wang. We thank Zane Martin for his helpful comments. We are thankful to all the authors for making their data available.

References

- Kikuchi, K., Wang, B., & Kajikawa, Y. (2012). Bimodal representation of the tropical intraseasonal oscillation. *Climate Dynamics*, 38(9–10), 1989–2000. <https://doi.org/10.1007/s00382-011-1159-1>
- Kiladis, G. N., Dias, J., Straub, K. H., Wheeler, M. C., Tulich, S. N., Kikuchi, K., et al. (2014). A comparison of OLR and circulation-based indices for tracking the MJO. *Monthly Weather Review*, 142(5), 1697–1715. <https://doi.org/10.1175/MWR-D-13-00301.1>
- Lawrence, D. M., & Webster, P. J. (2002). The Boreal Summer Intraseasonal Oscillation: Relationship between northward and eastward movement of convection. *Journal of the Atmospheric Sciences*, 59(9), 1593–1606. [https://doi.org/10.1175/1520-0469\(2002\)059<1593:TBSIOR>2.0.CO;2](https://doi.org/10.1175/1520-0469(2002)059<1593:TBSIOR>2.0.CO;2)
- Lee, J. Y., Wang, B., Wheeler, M. C., Fu, X., Waliser, D. E., & Kang, I.-S. (2013). Real-time multivariate indices for the Boreal Summer Intraseasonal Oscillation over the Asian summer monsoon region. *Climate Dynamics*, 40(1–2), 493–509. <https://doi.org/10.1007/s00382-012-1544-4>
- Lee, S.-S., & Wang, B. (2016). Regional Boreal Summer Intraseasonal Oscillation over Indian Ocean and Western Pacific: Comparison and predictability study. *Climate Dynamics*, 46(7–8), 2213–2229. <https://doi.org/10.1007/s00382-015-2698-7>
- Liebmann, B., & Smith, C. A. (1996). Description of a complete (interpolated) outgoing long-wave radiation dataset. *Bulletin of the American Meteorological Society*, 77, 1275–1277.
- Lin, H. (2013). Monitoring and predicting the intraseasonal variability of the East Asian–western North Pacific summer monsoon. *Monthly Weather Review*, 141(3), 1124–1138. <https://doi.org/10.1175/MWR-D-12-00087.1>
- Madden, R. A., & Julian, P. R. (1971). Detection of a 40–50 day oscillation in the zonal wind in the tropical Pacific. *Journal of the Atmospheric Sciences*, 28(5), 702–708. [https://doi.org/10.1175/1520-0469\(1971\)028<0702:DOADOI>2.0.CO;2](https://doi.org/10.1175/1520-0469(1971)028<0702:DOADOI>2.0.CO;2)
- Sabeerali, C. T., Ajayamohan, R. S., Giannakis, D., & Majda, A. J. (2017). Extraction and prediction of indices for monsoon intraseasonal oscillations: An approach based on nonlinear Laplacian spectral analysis. *Climate Dynamics*, 49(9–10), 3031–3050. <https://doi.org/10.1007/s00382-016-3491-y>
- Straub, K. H. (2013). MJO initiation in the real-time multivariate MJO index. *Journal of Climate*, 26(4), 1130–1151. <https://doi.org/10.1175/JCLI-D-12-00074.1>
- Suhas, E., Neena, J. M., & Goswami, B. N. (2013). An Indian monsoon intraseasonal oscillations (MISO) index for real time monitoring and forecast verification. *Climate Dynamics*, 40(11–12), 2605–2616. <https://doi.org/10.1007/s00382-012-1462-5>
- Wang, B., & Rui, H. (1990). Synoptic climatology of transient tropical intraseasonal convection anomalies: 1975–1985. *Meteorology and Atmospheric Physics*, 44(1–4), 43–61. <https://doi.org/10.1007/BF01026810>
- Wheeler, M. C., & Hendon, H. H. (2004). An all-season real-time multivariate MJO index: Development of an index for monitoring and prediction. *Monthly Weather Review*, 132(8), 1917–1932. [https://doi.org/10.1175/1520-0493\(2004\)132<1917:AARMMI>2.0.CO;2](https://doi.org/10.1175/1520-0493(2004)132<1917:AARMMI>2.0.CO;2)
- Zhu, B., & Wang, B. (1993). The 30–60-day convection seesaw between the tropical Indian and western Pacific Oceans. *Journal of the Atmospheric Sciences*, 50(2), 184–199. [https://doi.org/10.1175/1520-0469\(1993\)050<0184:TDCSBT>2.0.CO;2](https://doi.org/10.1175/1520-0469(1993)050<0184:TDCSBT>2.0.CO;2)